JOURNAL OF MATERIALS SCIENCE 21 (1986) 1647–1653

Crystallization of 3M/4X Mg–Si–Al–O–N melts

G. LENG-WARD, M. H. LEWIS
Department of Physics, Warwick University, Warwick, UK

S. WILD.
Department of Civil Engineering and Building, Polytechnic of Wales, UK

MgSiAlON 3M/4X liquids have been crystallized at slow cooling rates from the melt and isothermally at varying degrees of undercooling. Forsterite is always the primary crystallizing phase but the secondary phases vary with the degree of undercooling. A magnesium-substituted β'-sialon, β'', grows with forsterite via a coupled mechanism at a slow continous cooling rate. However, β'' is progressively replaced as the secondary phase by a petalite-type Mg–Si–Al–O–N phase and a fourth phase on isothermal crystallization at increasing degrees of undercooling. The compositions of β'' and Mg-petalite as analysed by energy-dispersive X-ray microanalysis are discussed.

1. Introduction

There is a continuing interest in phase equilibria and the development of microstructure in M–Si–Al–O–N systems in view of their relation to the oxynitride ceramics based on β'-Si_3N_4 and their potential as new refractory glass–ceramics. A number of studies have concentrated on the 3M/4X composition plane in the Mg–Si–Al–O–N system (where M = Mg + Si + Al and X = O + N) described by the general formula

$$Mg_{m/2}Si_{6-z+m/2}Al_{z-m}O_zN_{8-z} \quad (1)$$

This plane is bounded by the well known β' derivative solid solution of Si_3N_4, forsterite (Mg_2SiO_4) and spinel ($MgAl_2O_4$). It also contains a liquid-forming region [1] above a eutectic temperature of $\sim 1400°$ C (Fig. 1).

In the course of studying crystallization in glasses derived from liquids in the 3M/4X plane, Leng-Ward and co-workers [2, 3] have identified a new phase (β'') which has a phenacite-type crystal structure like β' but, unlike the latter, has a high solubility for magnesium. It is believed [2, 3] that β'' is a kinetically preferred metastable phase which crystallizes at low temperatures ($\sim 900°$ C) from parent glasses of similar composition. Decomposition of β'' occurs above 1120° C into the equilibrium forsterite phase together with other minor products. This metastable crystallization behaviour in oxynitride glasses is similar to that frequently observed within silicate glass–ceramics.

In this paper we present further observations of crystallization phenomena in the Mg–Si–Al–O–N system, concentrating on liquids in the 3M/4X plane which are slow-cooled from the melt rather than quenched before crystallizing heat-treatment. The study also provides an example of the use of the relatively new "windowless" energy-dispersive X-ray analysis for light elements in ceramic phases.

2. Experimental details

2.1. Materials preparation

Mg–Si–Al–O–N mixtures were prepared from high-purity SiO_2, Si_3N_4, Al_2O_3 and MgO powders. Compacted pellets were packed in boron nitride powder contained in a graphite crucible and reacted at 1600° C in a platinum-wound vertical tube furnace (nitrogen atmosphere). The liquid specimens were cooled either (i) at a slow continuous rate, or (ii) rapidly to a subsolidus temperature ($< 1420°$ C) which was maintained for 30 min before quenching. A 3M/4X eutectic liquid continuously cooled is referred to as "E", while a eutectic liquid cooled via an isothermal step at, say, 1325° C is referred to as "E1325".

2.2. Phase analysis.

Energy-dispersive X-ray microanalyses were obtained using (i) a JEOL JEM–100C transmission electron microscope (TEM/EDX) using thin-film correction factors to calculate quantitative Mg/Al/Si ratios, and (ii) a Cambridge scanning electron microscope (SEM/EDX) equipped with a "windowless detector" system suitable for light-element analysis. The light-element spectra were obtained using a very thin gold specimen coating, an accelerating voltage of 8kV and with the beryllium detector window replaced by a thin organic window.

The quantitative analysis of oxygen and nitrogen from X-ray emission spectra is inhibited by their sensitivity to absorption and other correction factors. The windowless energy-dispersive X-ray spectra exemplified in this work enable a quantitative analysis of light-element containing phases by combining the nitrogen/oxygen (N/O) ratios obtained by comparison with standards with the quantitative TEM magnesium/aluminium/silicon (Mg/Al/Si) data obtained with a beryllium window in position. The standards used to obtain a range of nitrogen/oxygen EDX profiles are

0022–2461/86 $03.00 + .12

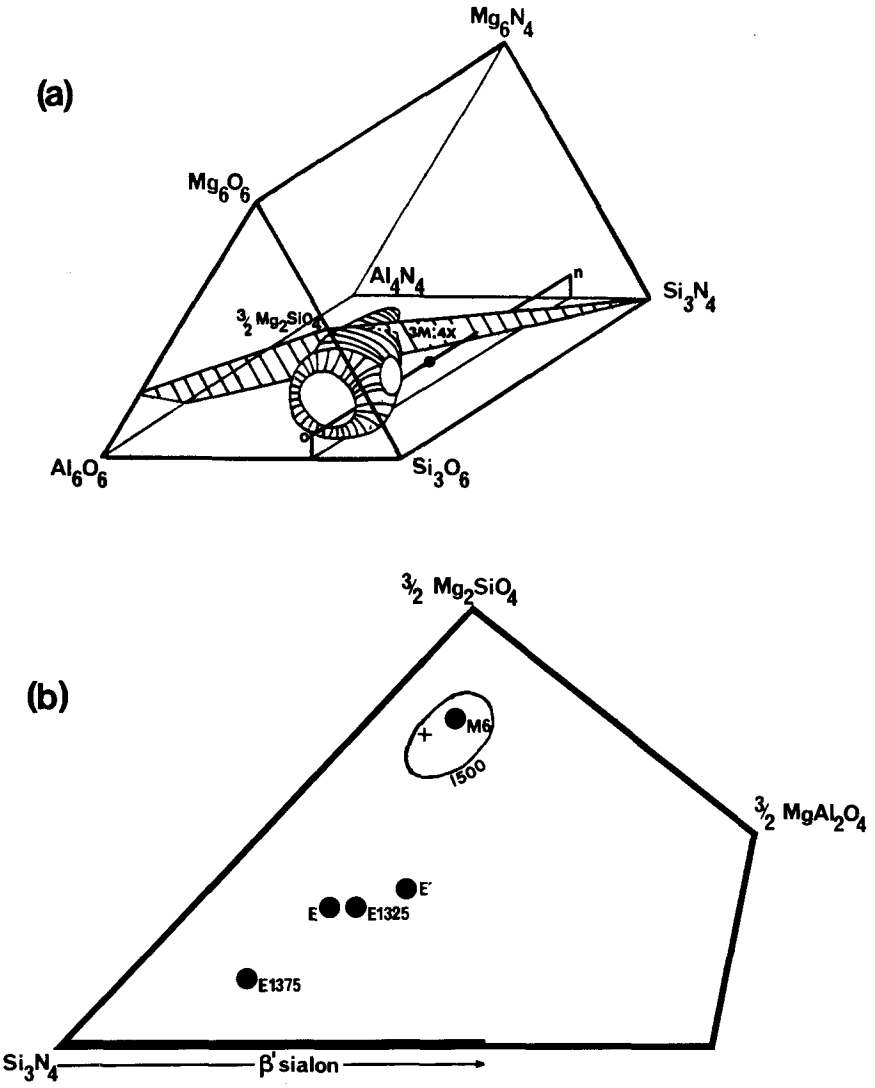

Figure 1 (a) Glass-forming region and 3M/4X plane of Mg–Si–Al–O–N system (from Drew *et al.* [1]). (b) Mg–Si–Al–O–N 3M/4X composition plane (+ 3M/4X eutectic).

(a) Si_2N_2O, (b) $\beta'SiAl_2ON$, (c) an intimate equimolar mixture of pressed AlN and SiO_2 powders, (d) a glass of nominal composition $Y_{1.03}Si_{1.26}Al_{1.26}O_{4.2}N_{1.2}$ and (e) Mg_2SiO_4. These five profiles (shown below in Fig. 8) are of compositions with N/O ratios of respectively 2, 1, 0.5, ~0.28, and 0.

The Y–Si–Al–O–N glass composition (d) is included as an example of an oxynitride glass containing close to the maximum possible level of nitrogen. The N/O profile of crystalline N-wollastonite, $Y_2Si_2O_4N_2$, was checked and found to be not significantly different from the equimolar AlN:SiO_2 mixture.

3. Microstructural analysis

3.1. Continuously cooled liquids

The 3M/4X eutectic MgSiAlON liquid crystallized into a duplex mixture of forsterite and β'' during cooling at a rate of approximately $10°C\,min^{-1}$. Cooling rates appreciably faster inhibited complete crystallization. The microstructure consists of elongated skeletal forsterite crystals together with large volumes (~80%) of duplex forsterite/β'' microstructure in the eutectic morphology shown in Fig. 2a. The specimen is porous as a result of solidification shrinkage and/or some gas evolution. SEM micrographs (Figs. 2b and c) of the etched duplex structure show that the hot HCl acid etch dissolves the forsterite in preference to β''. A TEM micrograph of the duplex structure is shown in Fig. 3a together with an electron diffraction pattern in Fig. 3b. The $(1\,2\,\bar{5})$ zone pattern of the hexagonal β'' is visible between the broken lines along with the orthogonal (1 0 0) forsterite spot pattern. Figs. 3c and d show TEM/EDX analyses of the duplex forsterite and β'' phases crystallized from a 3M/4X liquid.

Fig. 3e shows a β'' analysis from the duplex structure of a liquid of higher aluminium content than the eutectic composition. Such liquids with compositions a short way from the 3M/4X eutectic towards $MgAl_2O_4$ also crystallize into a duplex forsterite/β'' product but with the β'' phase of increased aluminium, magnesium and oxygen substitution.

3.2. Quenched and isothermally crystallized liquids

Specimen E1400 consists of elongated skeletal forsterite crystals in a glass matrix. A section through such a crystal in Fig. 4 shows a combination of planar faces, smooth curved lobes and re-entrants (hopper shaped).

Specimen E1375 partially crystallized into an intimate mixture of elongated skeletal forsterite crystals and β'' as shown in the back-scattered mode SEM micrograph of Fig. 5a. The light-contrast β'' crystals have sporadically nucleated at the forsterite–liquid interface and grown into the liquid, and are partially

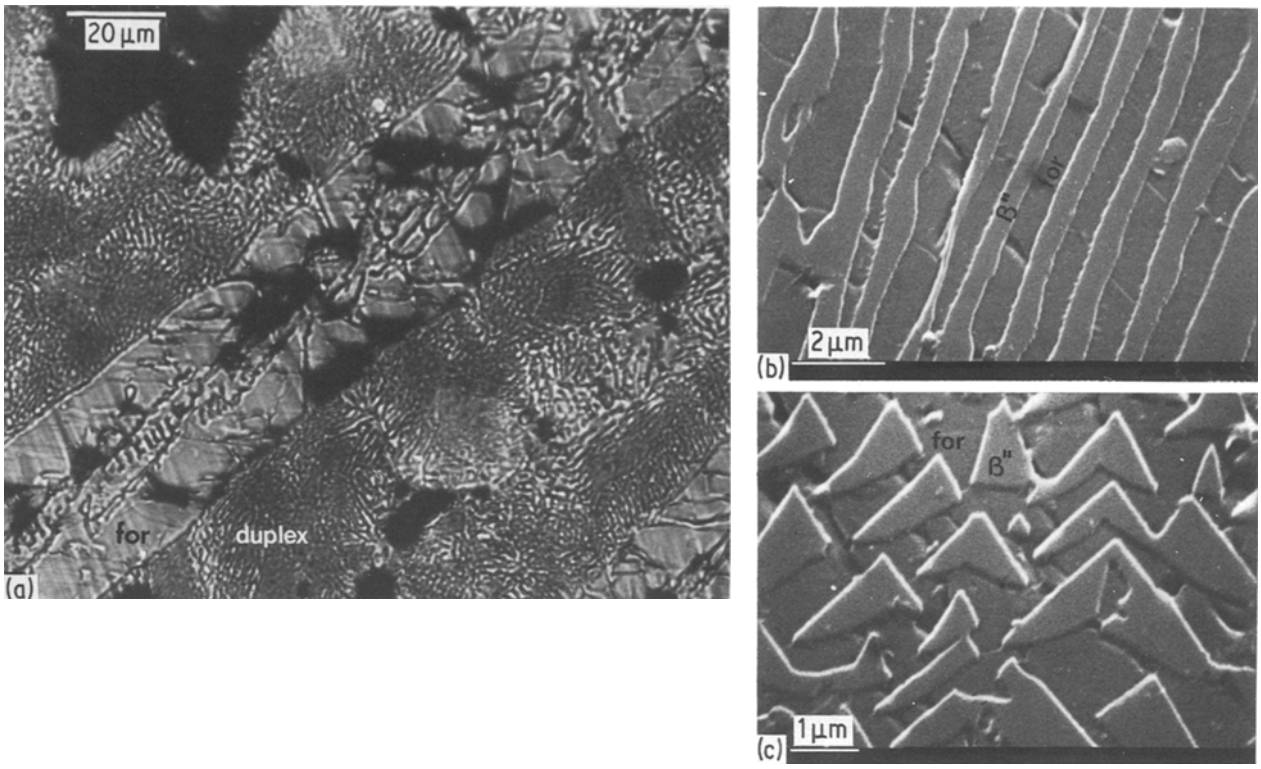

Figure 2 Micrographs of duplex forsterite/β'' microstructure: (a) optical (reflected light), (b, c) SEM, etched with 1% HF.

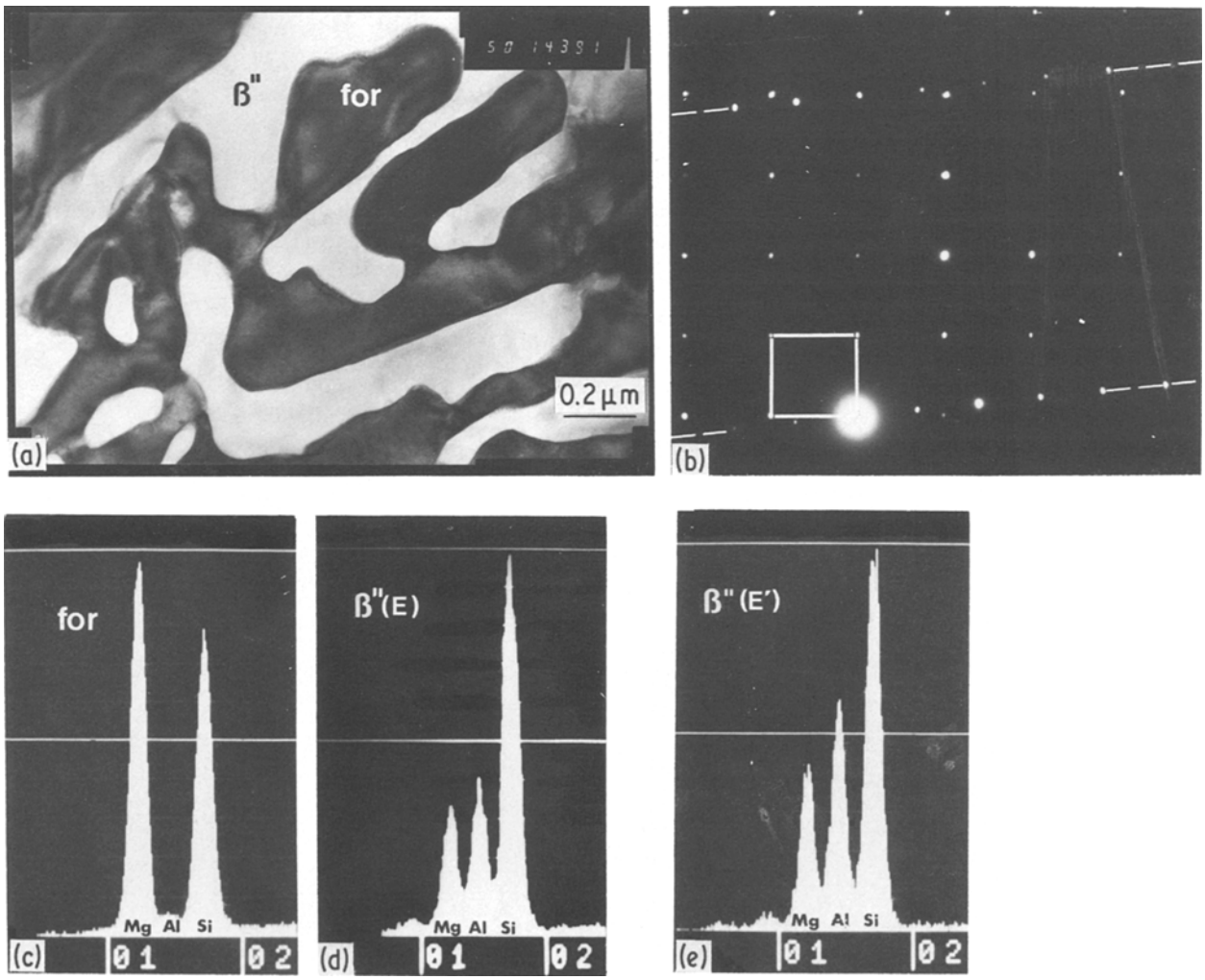

Figure 3 (a) TEM micrograph of duplex forsterite/β'' microstructure with (b) associated electron diffraction pattern. TEM/EDX analyses of (c) forsterite, (d) β''(E) and (e) β'' (E′).

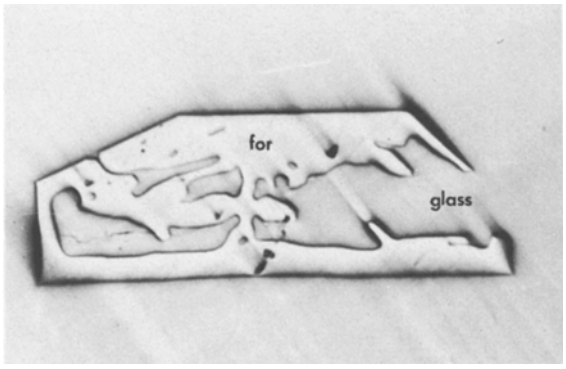

Figure 4 Optical micrograph (reflected light) of E1400.

or completely surrounded by forsterite (dark contrast). Severe cracking has occurred within the forsterite crystals on cooling. SEM/EDX analyses of these two crystalline phases are shown in Figs. 5b and c.

Specimen E1325 crystallized into forsterite, β'', Mg-petalite, and traces of a fourth unknown phase termed Q. The main three crystalline phases in E1325 are easily identified in the TEM since the forsterite contains electron radiation damage giving it a mottled appearance, the Mg-petalite has a tabular morphology with crystal stacking faults and the β'' crystals are featureless (Fig. 6a). Both SEM/EDX and TEM/EDX analyses of the β'' and Mg-petalite phases are presented in Figs. 6c and d.

The Mg-petalite is so termed because of the characteristic triplet around the d spacing of 0.36 nm among the five lines positively identified as part of its powder X-ray diffraction pattern (0.361 nm (m), 0.358 nm (m), 0.353 nm (s), 0.291 nm (w), 0.283 nm (w), 0.243 nm (w)). X-ray diffraction patterns of this type are known [4] for the structurally related monoclinic natural mineral petalite ($LiAlSi_4O_{10}$) and the orthorhombic synthetic lithium disilicate $Li_2Si_2O_5$. The three reciprocal lattice unit cell dimensions a', b' and c' outlined in the Mg-petalite electron diffraction patterns of Fig. 6b correspond to orthorhombic unit cell

TABLE I Orthorhombic unit cell dimensions

Phase	a (nm)	b (nm)	c (nm)
Mg-petalite	0.558	1.415	0.496
A*	0.5581	1.4136	0.4942
B*	0.5628	1.4328	0.4969
C*	0.5582	1.4158	0.4944
$Li_2Si_2O_5$	0.580	1.466	0.4806
$LiAlSi_4O_{10}$	2 × 0.588	1.405	0.514

*From Mah [5].

dimensions of $a = 0.558$ nm, $b = 1.415$ nm and $c = 0.496$ nm. These unit cell dimensions are listed in Table I, together with those for compounds designated A, B and C by Mah [5] for a similar phase called the "N-phase", and also for $Li_2Si_2O_5$ and the pseudo-orthorhombic unit cell dimensions of mineral petalite.

Specimen E1100 crystallized into a fine dendritic forsterite structure with a mixture of Mg-petalite and unknown Q phase in the interdendritic region (Fig. 7). Trace amounts of β'' are present. The Q phase crystals have not been characterized in this work as there are only a few diffuse powder X-ray diffraction lines attributable to the Q phase, and a small enough TEM/EDX microanalysis probe was not available to get specific analyses on the small, faulted Q phase crystals.

The analysed compositions and unit cell dimensions of four "low magnesium" β'' phases are presented in Table II and plotted on the 3M/4X plane in Fig. 1b. These four β'' phases are β'' (E) from the slow-cooled eutectic liquid, β'' (E′) from the slow-cooled aluminium-rich liquid, β'' (E1375) and β'' (E1325). For comparison the compositions of a "high magnesium" β'' (M6), $z = 4$ β'-sialon and β-Si_3N_4 are also shown. The oxygen/nitrogen compositions for these β'' phases are calculated from Formula 1 knowing the analysed Mg/Si/Al levels.

4. Discussion

4.1. Crystallization mechanisms

In previous publications we have described the crystallization of the metastable β'' phase from quenched

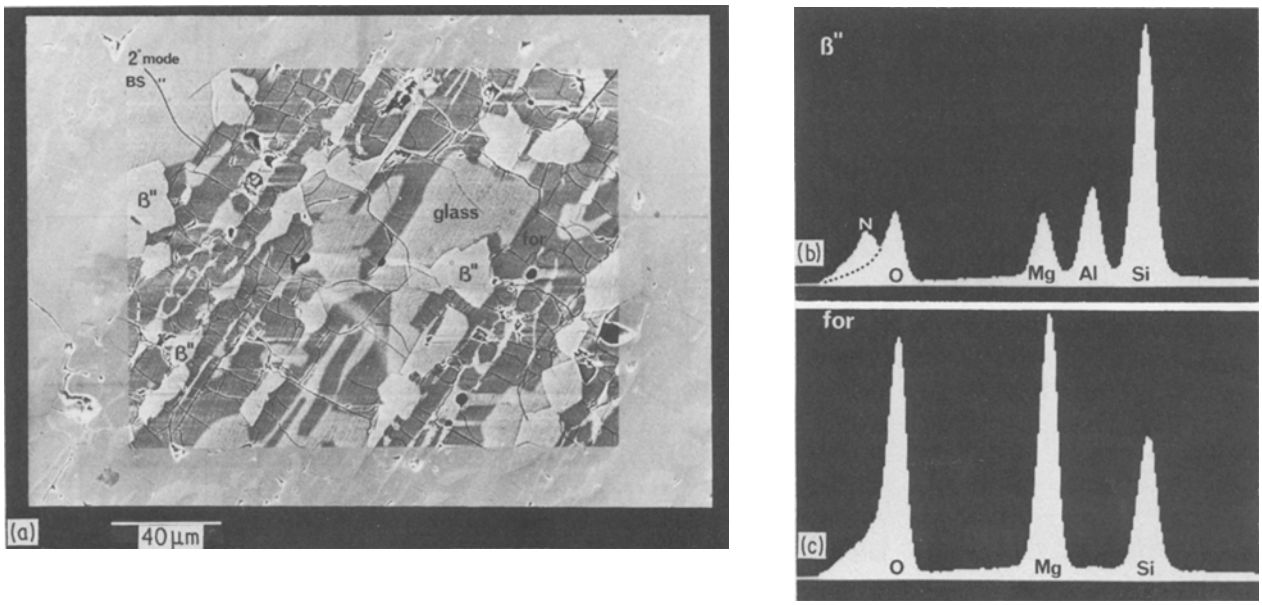

Figure 5 (a) SEM micrograph of E1325 (secondary and back-scattered electron mode), and SEM/EDX analyses of (b) β'' and (c) forsterite.

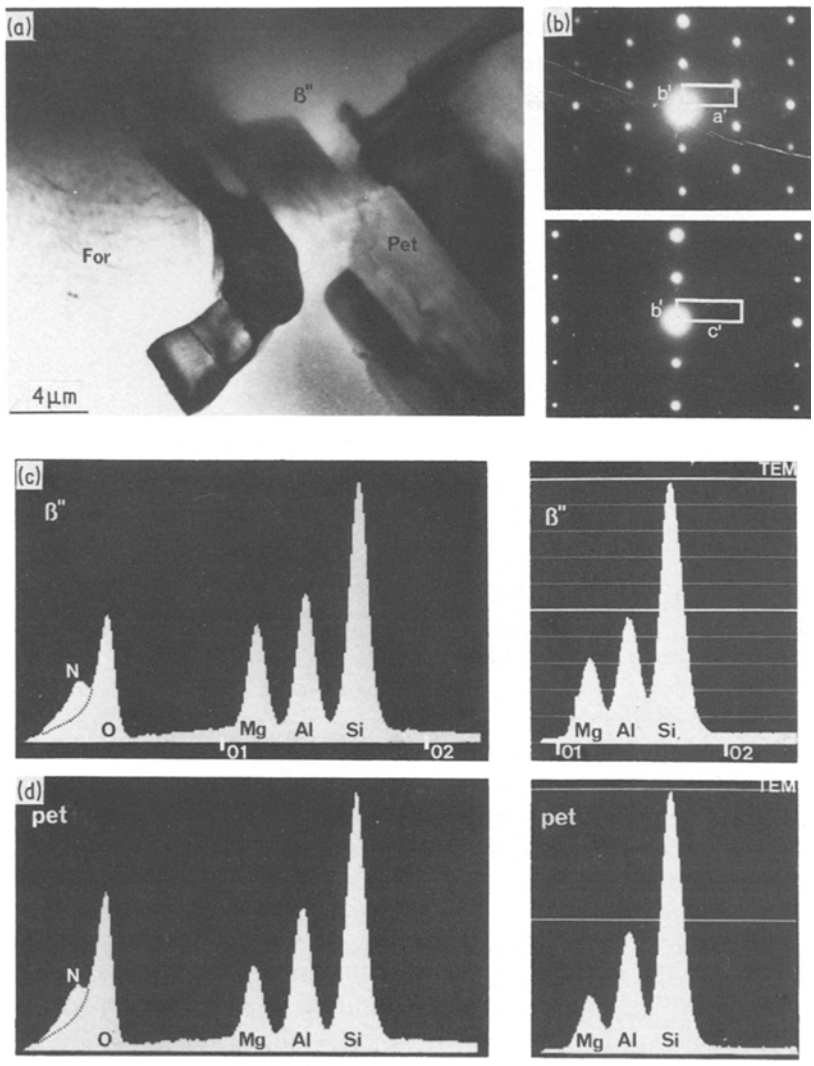

Figure 6 E1375 (a) TEM micrograph, (b) electron diffraction patterns from Mg-petalite phase. SEM/EDX and TEM/EDX analyses of (c) β'' and (d) Mg-petalite.

near-eutectic liquids in the 3M/4X plane when annealed below 1000° C. Similar compositions studied in this work also exhibit metastable crystallization products, but at higher temperatures this is preceded by crystallization of the equilibrium forsterite (Mg_2SiO_4) phase which influences both the morphology and the composition of the metastable products.

On cooling from above the liquidus and holding at a low level of undercooling (E1400), forsterite crystals initially grow with a faceted anisotropic morphology typical of silicate crystallization near to the liquidus temperature. The segregation of insoluble aluminium and nitrogen together with excess silicon at the interface between forsterite and the increasingly viscous liquid produces cellular projections, due to constitutional supercooling, on those interfaces at the forsterite plate periphery which have a relatively small anisotropy in the solid–liquid interfacial energy. The resulting morphology is typified by the "hopper" shaped two-dimensional section through a forsterite crystal in Fig. 4.

Forsterite crystallization is suppressed by the progressive enrichment of the residual liquid in aluminium, nitrogen and excess silicon. This residual liquid under equilibrium conditions would be expected to crystallize mainly as a highly substituted β' at a composition on the tie-line from Mg_2SiO_4 through the eutectic liquid composition (Fig. 1b). However, nucleation and growth of the metastable β'' phase is kinetically favoured under conditions of moderate residual magnesium content and a sufficient degree of undercooling for nucleation to take place, and at much lower temperatures than for β'

TABLE II β'' analyses and hexagonal unit cell dimensions

Phase	Mg	Si	Al	O*	N*	a (nm)	c (nm)	c/a
β'' (M6)	3.2	2.2	0.6	7.1	0.9	0.7875(3)	0.3105(4)	0.3943(5)
β'' (E′)	1.7	2.5	1.9	5.2	2.8	0.7745(5)	0.3030(7)	0.391(1)
β'' (E1325)	1.5	2.9	1.6	4.6	3.4	0.7725(5)	0.3015(7)	0.390(1)
β'' (E)	1.6	3.0	1.4	4.6	3.4	0.7722(5)	0.3012(7)	0.390(1)
β'' (E1375)	0.9	3.8	1.3	3.1	4.9	0.7704(5)	0.3007(7)	0.390(1)
β' (z = 4)		2.0	4.0	4.0	4.0	0.7712(3)	0.3004(2)	0.3895(3)
β-Si_3N_4		6.0			8.0	0.7604(4)	0.2908(2)	0.3824(4)

*Calculated using Formula 1.

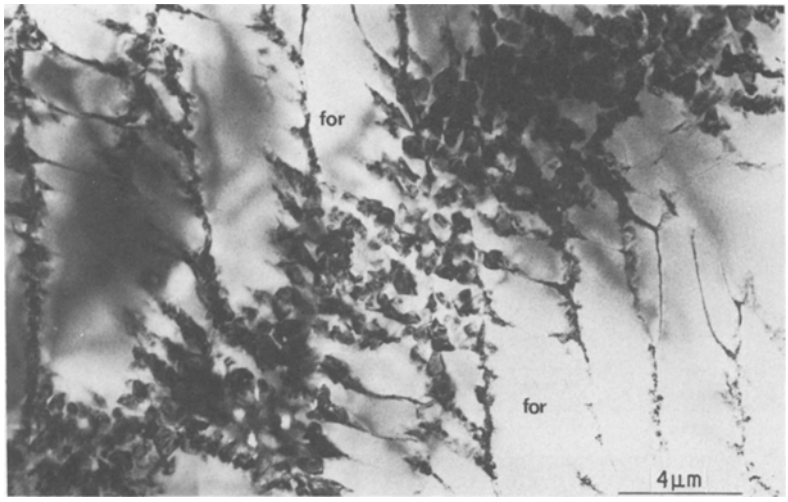

Figure 7 TEM micrograph of E1100.

precipitation during liquid-phase sintering of β' ceramics. This is illustrated by the crystallization of β'' together with forsterite in E1375 (Fig. 5) and in the continuously cooled eutectic specimen E (Figs 2 and 3).

The crystallization morphology and composition of β'' is a function of the volume fraction and morphology of the equilibrium forsterite which precedes it. In continuously cooled specimens β'' crystallizes from a large residual liquid volume in a duplex eutectic morphology with forsterite. The microstructural regularity, of constant interlamellar spacing in many areas (Fig. 2b), indicates a coupled growth of metastable β'' and equilibrium forsterite at a nearly isothermal interface.

On quenching from above the liquidus to a much reduced isothermal crystallization temperature and a higher degree of undercooling, as for E1100, there is a more severe segregation of elements insoluble in forsterite into the residual liquid together with higher liquid viscosities. The forsterite interfaces degenerate into the cellular/dendritic morphology exemplified in E1100 (Fig. 7), and this prevents the extensive development of a regular eutectic morphology, Under these conditions the β'' phase is almost completely replaced by alternative metastable phases, Mg-petalite and Q phase, of similar composition but which may be kinetically preferred at the lower temperature. In E1325, held at a medium isothermal hold temperature, a mixture of all three secondary phases, β'', Mg-petalite and Q crystallize together with forsterite.

4.2. Metastable phase compositions

The β'' phases in E, E', E1375 and E1325 have lower magnesium substitution levels and consequently smaller lattice parameters than for β'' crystallizing from a near-eutectic liquid (M6 in Fig. 1b, Table I and Wild *et al.* [2]). This is consistent with the expansion of β'' lattice parameters with magnesium substitution (Table I). It is believed that the low-temperature limit for decomposition of metastable β'' is linked to the substitution level of the comparatively large magnesium atom, that for composition M6 being $\sim 1120°$ C compared to crystallization temperatures above 1300° C for β'' which accompanies forsterite.

The N/O profile of the SEM/EDX spectra of β'' (E1325) in Fig. 6c is shown as a dashed line in Fig. 8. It lies midway between the curves labelled 1 : 1 and 0.5 : 1, which is consistent with the N/O ratio of 0.74 (3.4/4.6) calculated from the Mg/Al/Si ratio analysed by TEM/ EDX and the 3M/4X composition formula (Table II).

The Mg-petalite phase in E1325 has a similar Al/Si ratio to the β'' (E1325) phase but a lower magnesium level and a higher value of O/N (Fig. 6c). This means that its composition must lie just below the 3M/4X plane. A line of constant Mg/Al/Si level (0.63/1.00/1.95) corresponding to the analysed TEM/EDX Mg-petalite composition is shown drawn from the oxide face (o) to the nitride face (n) of the Mg–Si–Al–O–N triangular prism in Fig. 1a. The Mg-petalite N/O profile lies very close to the 0.5 : 1 standard, and so the overall analysed Mg-petalite composition is $Mg_{0.63}Al_{1.00}Si_{1.95}O_{3.4}N_{1.7}$. This composition lies between the 3M/4X plane and the

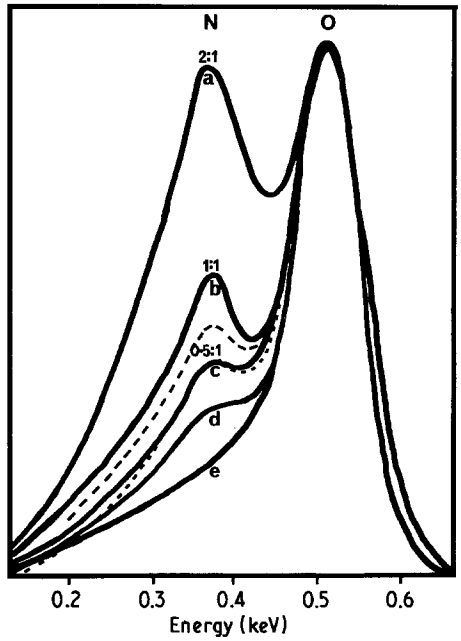

Figure 8 Nitrogen/oxygen profiles of (a) Si_2N_2O, (b) β'-$SiAl_2ON$, (c) SiO_2 + AlN, (d) $Y_{1.03}Si_{1.26}Al_{1.26}O_{4.2}N_{1.2}$ glass, and (e) Mg_2SiO_4. (– – –) petalite, (———) β'' (E1325).

liquid-forming region as shown by the black dot on the line o–n in Fig. 1a.

The similarity in unit cell dimensions between Mg-petalites and the three examples of Mah's N phase is evidence for them being the same phase, and shows that this phase occurs over at least a short range of composition. The Mg/Al/Si composition of the Mg-petalite found in this work is consistent with Mah's observation [5] of N phase occurring in equilibrium with a glassy phase of similar Mg/Al/Si ratio, $Mg_{0.71}Al_{1.18}Si_{1.77}O_{4.24}N_{1.18}$. However, Mah's suggested formula for N phase of Mg_2AlSiO_4N has a much higher magnesium level and lower silicon level than that analysed in this work.

The nitrogen-containing Mg-petalite composition found in this work lies approximately midway between the following two possibilities derived from the mineral petalite and lithium disilicate compositions. The replacement of lithium and some silicon in the formula of mineral petalite, $LiAlSi_4O_{10}$, to give the Mg-petalite Mg/Al/Si ratio analysed in this work while maintaining the mineral's 6/10 cation/anion ratio, gives the oxide composition $Mg_{0.63}Al_{1.00}Si_{1.95}O_6$. Lithium silicate, $Li_2Si_2O_5$, has a very similar structure to mineral petalite [4] and the replacement of lithium, some silicon and oxygen to give the analysed Mg-petalite Mg/Al/Si ratio while maintaining an 8/10 cation/ratio gives the oxynitride composition $Mg_{0.63}Al_{1.00}Si_{1.95}O_{1.5}N_3$. Further work is needed to rationalize the nitrogen-containing Mg-petalite's composition range and its structural relationship to mineral petalite and $Li_2Si_2O_5$.

The structure and composition range of Mg-petalite phases prepared from oxide glasses are also yet to be properly resolved. Mg-petalite has been prepared from oxide glasses as a metastable phase, but (as in this work) always in combination with other crystalline phases. Schrayer and Schairer [6] suggested the formula $MgAl_2Si_3O_{10}$ for the Mg-petalite phase that they observed together with cordierite, quartz, and pyroxene in annealed glasses. However, neither Schrayer and Schairer [6] nor Schulz *et al.* [7] obtained Mg-petalite in annealed glasses prepared at exactly this composition.

5. Conclusions

The crystallization of metastable oxynitride phases from nitrogen-containing liquid/glass mixtures parallels that frequently observed in silicate glass–ceramics. They are normally kinetically preferred due to a compositional similarity to the parent glasses, and to the inhibition of the large diffusional composition changes required for equilibrium phases. In the work described here they are oxynitrides (β'', Mg-petalite and Q) which accompany the crystallization of a pure silicate–forsterite, in preference to β'.

The β'', which has been structurally and compositionally analysed in previous work [2, 3], is observed in this research with lower and variable magnesium content when accompanied by forsterite. Although not structurally defined, the composition of the additional metastable petalite phase has been determined by energy-dispersive X-ray analysis. This has provided an example of the use of a relatively new "windowless" X-ray detector for O/N analysis using a range of oxynitride standards.

References

1. R. A. L. DREW, S. HAMPSHIRE and K. H. JACK, in "Progress in Nitrogen Ceramics", edited by F. L. Riley (Martinus Nijhoff, The Hague, 1983) p. 323.
2. S. WILD, G. LENG-WARD and M. H. LEWIS, *J. Mater. Sci.* **16** (1981) 1815.
3. G. LENG-WARD, M. H. LEWIS and S. WILD, *ibid.* **19** (1984) 1726.
4. F. LEIBAU, *Acta Cryst.* **14** (1961) 389.
5. T. MAH, PhD Thesis, Ohio State University (1976).
6. W. SCHRAYER and J. F. SCHAIRER, *Amer. Miner.* **17** (Jan/Feb 1962) 90.
7. H. SCHULZ, G. M. MUCHLOW, W. HOFFMAN and G. BAYER, *Z. Krist.* **133** (1971) 91.

Received 30 May
and accepted 4 July 1985